PERGAMON

International Journal of Heat and Mass Transfer 41 (1998) 3075–3085

International Journal of HEAT and MASS TRANSFER

Influence of fuel-side heat loss on diffusion flame extinction

Anjan Ray*†, Indrek S. Wichman

Department of Mechanical Engineering, Michigan State University, East Lansing, MI 48824, U.S.A.

Received 15 July 1997; in final form 27 December 1997

Abstract

The influence of a fuel-side heat loss zone on a diffusion flame established between fuel and oxidizer reservoirs is investigated using a model heat loss profile. The radiative heat loss suffered by a flame due to particulate soot served as the background motivation for this study. For each chosen flame, the intensity, width and location of the heat loss profile were parametrically varied to assess the sensitivity of the flame to heat losses. The influence of such variations on the heat release, the heat flux to the reservoir walls, the radiative fraction and the drop in flame temperature was studied. Emphasis was placed on the phenomenon of flame extinction due to increased heat losses. Extinction plots were generated for a range of fuel and oxidizer reservoir mass fraction values. The influence of the losses is characterized best by the integrated value of the heat loss profile. In all situations studied, the temperature and reactivity peaks moved toward the fuel side with increased heat losses.

Nomenclature

a_p Planck mean absorption coefficient
A pre-exponential factor
b reduced Damköhler number
b^* reduced Damköhler number with zero heat losses
c_p specific heat
D_O, D_F diffusion coefficients for oxidizer, fuel
$\mathbf{D}$ Damköhler number; $\mathbf{D} = t_{ref}/t_{chem}$
$\mathbf{D}$ modified Damköhler number defined as the quantity in square brackets in equation (6)
$\mathbf{D}_E$ Damköhler number at extinction
$\mathbf{D}^*$ Damköhler number without heat losses
E activation energy for the chemical reaction
f_v soot volume fraction
h rescaled enthalpy defect, $h = \beta|H(Z)|$
H enthalpy defect, $H = \tau + y_O + y_F - 1$
L distance between fuel and oxidizer walls
N_R radiation number, $N_R = q_{R,ref}/[\lambda_o(T_f - T_o)/L]$
$\mathbb{N}_R$ modified radiation number, $\mathbb{N}_R = (N_R \Delta Z_R) Z_f (1-\theta/2)\beta C(Y_{OO})$
$\bar{q}_R$ nondimensional radiant energy flux, $\bar{q}_R = q_R/q_{R,ref}$
q_{Rad} integral of the heat loss term, $q_{Rad} = \int_0^1 (N_R)\mathrm{sech}^2 B(Z - Z_R)\mathrm{d}Z$
q_{total} integrated heat release, $q_{total} = \int_0^1 (1+\phi)\mathbf{D}r\mathrm{d}Z$
Q_F heat release per unit mass of fuel
$\bar{Q}_F$ nondimensional heat release, $\bar{Q}_F = Q_F Y_{FF}/[C_p(T_f - T_o)] = 1 + \phi$
$Q_{W,O,cond}$ heat flux by conduction to the oxidizer wall
$Q_{W,O,rad}$ heat flux by radiation to either wall, $Q_{W,O,rad} = 0.5\int_0^L (\mathrm{d}q_R/\mathrm{d}x)\mathrm{d}x$
r nondimensional reaction term, $r = y_O y_F \exp[-\beta(1-\tau)/[1-\alpha(1-\tau)]]$
R universal gas constant
s, s_o mass coordinate, $s = \int_0^x \rho \mathrm{d}x$, $s_o = \int_0^L \rho \mathrm{d}x$
$\bar{s}$ nondimensional mass coordinate, $\bar{s} = s/s_o$
t_{ref} characteristic diffusion time, $t_{ref} = L^2/\alpha_o$
t_{chem} $t_{chem} = 1/[A Y_{OO} \exp(-E/RT_f)]$
$\bar{t}$ $\bar{t} = t/t_{ref}$
T temperature
T_f adiabatic flame temperature, $T_f = T_o + Q_F Y_{FF}/[C_p(1+\phi)]$
$U(Z)$ heaviside step function
w reaction term, $w = \rho A Y_O Y_F \exp(-E/RT)$
x spatial coordinate

* Corresponding author. Tel.: (517) 353-9180; fax: (517) 353-1750; e-mail: wichman@egr.msu.edu, raya@mech.iitd.ernet.in.

† Current address: Department of Mechanical Engineering, Indian Institute of Technology, Delhi, Hauz Khas, New Dehli, 110016, India.

0017-9310/98 $19.00
PII: S0017-9310(98)00028-3

$\bar{x}$ nondimensional spatial coordinate, $\bar{x} = x/L$
y_F, y_O rescaled fuel, oxidizer mass fractions, $y_F = Y_F/Y_{FF}$, $y_O = Y_O/Y_{OO}$
Y_F, Y_O fuel, oxidizer mass fractions
Z physical coordinate, $Z = 1 - \bar{s}$; also the mixture fraction
Z_f Burke–Schumann or IRR flame location, $Z_f = 1/(1+\phi)$
Z_{R+}, Z_{R-}, Z_R Z-values at right, left, middle of radiation-loss zone. Z_{R-} is closest to the flame sheet, Z_{R+} is furthest from the flame sheet.

Greek symbols
α $\alpha = 1 - T_o/T_f$
β Zeldovich number, $\beta = \alpha E/RT_f$
ΔZ_R radiation-loss zone thickness, $\Delta Z_R = Z_{R+} - Z_{R-}$
θ sum of Z_{R+} and Z_{R-}, $\theta = Z_{R+} + Z_{R-}$
λ thermal conductivity
ν mass-based stoichiometric coefficient for the reaction $F + \nu O \rightarrow (1+\nu)P$
ρ density
$\bar{\rho}$ nondimensional density, $\bar{\rho} = \rho/\rho_o$
σ Stefan–Boltzmann constant
τ nondimensional temperature, $\tau = (T - T_o)/(T_f - T_o)$
ϕ global equivalence ratio, $\phi = \nu Y_{FF}/Y_{OO}$.

Subscript
R in radiant-loss zone.

Abbreviations
BS Burke–Schumann
IRR infinite reaction rate.

1. Introduction

The interaction between a diffusion flame and a nearby heat loss zone is complex. Often, the heat losses are produced by radiation from a fuel-side soot layer. Soot is formed in a diffusion flame as a consequence of a complicated chain of physical and chemical processes. There are uncertainties in the description of soot processes in a flame. Soot formation mechanisms are not completely understood. In this article, we investigate the influence of a fuel-side heat loss profile on a pure diffusion flame established between two infinite, porous walls. In particular we examine the 'sensitivity' of a 'given' primary reaction zone (flame) to imposed variations of the heat loss profile, such as its intensity, width and location. Flame extinction conditions are studied in detail. It has to be mentioned at the outset that the assumed loss zone need not necessarily originate due to a soot layer. For example, the losses may arise from a radiating porous grid placed next to the flame. Thus, our model describes general features of diffusion flames with heat losses, with special emphasis on extinction conditions.

The influence of radiative losses on diffusion flames has received significant attention in recent years, see the extensive reviews of refs. [1, 2]. Thermal radiation from a flame can occur from the gases (H_2O, CO_2) at high temperature [2], and the combustion-generated particulates, i.e. soot. According to the calculations of Grosshandler and Modak [3], for soot volume fractions greater than 10^{-7}, soot radiation is dominant. If soot radiation overwhelms gaseous radiation from CO_2, H_2O and other species [2], the neglect of gaseous radiation becomes a modeling option.

In a diffusion flame the characteristic transport time is greater than the characteristic chemical reaction time, unless the flame is near extinction. Some characteristics of diffusion flames have been discussed [4], including the detailed nature of the temperature and reaction rate profiles. It was observed that the maximum reaction rate usually will not coincide with the temperature maximum. The only exception is the symmetric flame for which the overall stoichiometric coefficient, ϕ, equals unity. For $\phi > 1$ the peak of the reaction rate lies between the Burke-Schumann flame location and the peak of the temperature profile. Identical conditions apply when $\phi < 1$. This predicted behavior has been verified in DNS simulations of turbulent diffusion flames [5]. The implication of these observations is that it is the reactivity peak that is important for flame behavior, not the temperature peak, though the latter is much more easily measured.

In the thin-flame limit [6] all diffusion flames are 'non-convective' diffusion flames because the mixture fraction transformation eliminates the convective term while producing the dominant reactive–diffusive balance $T_{zz} \approx \mathbf{D}|\underset{\sim}{\nabla} Z|^{-2} w$. However, $|\underset{\sim}{\nabla} Z|$ depends strongly on the heat and fluid flow conditions and it introduces a new function which depends on the spatial coordinates and the time. The mixture fraction gradient may be absorbed into a suitably defined Damköhler number $\tilde{\mathbf{D}} \equiv \mathbf{D}|\underset{\sim}{\nabla} Z|^{-2}$ in front of w. Its functional dependence must, of course, be withdrawn when later conducting a full examination of the problem. At this withdrawal stage, the spatial and transient nature of $|\underset{\sim}{\nabla} Z|$ exerts its influence.

Our goal is to describe the response of a diffusion flame to soot-like radiant energy losses. We shall examine the total flame heat flux, the total (conductive plus radiative) energy flux to the lateral porous walls, and the drop in flame temperature due to radiant loss. Most importantly, we shall investigate the variation in the radiative fraction values with parametrically varied heat loss zones.

We emphasize that the practical aim of this research has been to examine possible self-extinguishment of diffusion flames in microgravity. The absence of buoyancy-generated convection of hot particulates (soot) from the vicinity of the reaction zone suggests that radiative losses from the particulates might depress flame temperatures sufficiently to cause self-extinction. The research literature of combustion contains few studies

wherein descriptions of both soot formation and radiation are included.† The studies that reintegrate certain results of basic soot research into flame theory are generally detailed simulations for specific configurations [7–12]. Agreement between computations and experiments is attained by adjusting simulation parameters. Detailed sensitivity analyses [13, 14] of the kind that support parametrically based simulations are, to the knowledge of the authors, never conducted.

A simulation is useful when the physical configuration is of direct interest, when the theory in question is understood beyond doubt and when no processes have been excluded. Difficulties occur when physical processes are ignored. For example, rigorous continuum-mechanical theories [15] clearly state that multicomponent reactive media generally possess multiple temperatures. Nowhere in combustion can this be more relevant than in the case of a soot–gas mixture. Yet in only very few of the existing soot studies does the notion of multiple temperatures enter the formulation [16, 17]. Interestingly, [16], which examines carbon particle ignition, concludes that "... the effects of surface radiative loss are shown to be significant for isolated particle burning." Hence, having a correct particle surface temperature is imperative for producing accurate radiation-field estimates.

Our model, by contrast, makes no such restrictions. If a means can be found for relating multiple temperatures—or any other physical effect—to the heat loss zone width, displacement and amplitude, then that effect is by definition included in the analysis.

2. The model

Figure 1 schematically depicts the problem geometry. The fuel and the oxidizer diffuse through walls located at $x = 0$ and $x = L$, respectively. A diffusion flame is established between the two walls. A soot layer exists initially on the fuel side of the theoretical DF location, consistent with experimental observations [18]. The walls have ambient temperature T_o. There is no fuel in the oxidizer stream and no oxidizer in the fuel stream. This configuration is canonical, because all diffusion flame problems qualitatively resemble it, whether (i) porous spheres, (ii) burning droplets, (iii) counterflow flames, (iv) jet flames, (v) flame spread, etc. All of these configurations, however, contain complicating spatial variations that do not enhance our qualitative understanding. Some configurations are inherently unsteady, e.g. (ii). In (i)–(iii) the equations contain variable coefficients whereas (iv) and (v) are irreducibly two-dimensional. Of the above configurations, ours is the easiest to examine.

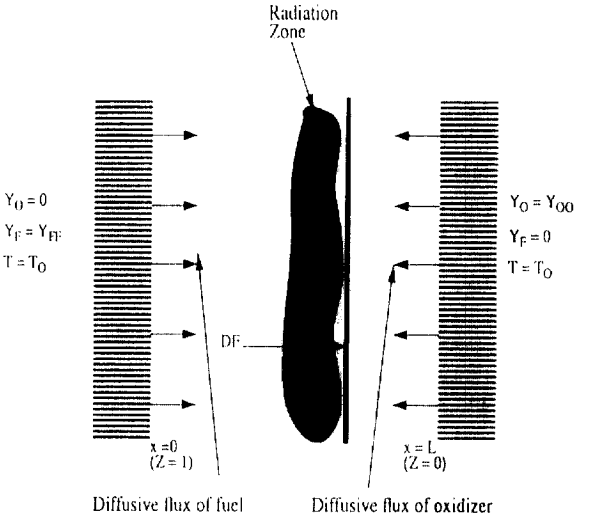

Fig. 1. The problem geometry, including the diffusion flame (DF), the radiation (soot) zone and the porous diffusive walls at $x = 0$ and $x = L$.

The combustion occurs through a global, one-step mass-based reaction of the form $F + \nu O \rightarrow (1+\nu)P$. A hydrocarbon is nominally the fuel under consideration and oxygen is the oxidizing species. A suitable set of parameter values must be used to generate a range of Damköhler numbers and flame temperatures. The theoretically defined adiabatic flame temperature (see Nomenclature) produces unrealistically high adiabatic flame temperatures. A set of realistic hydrocarbon combustion flame temperatures was obtained from the experimental work on flame spread over solid fuels by Ray [19] and Fernandez-Pello et al. [20], as tabulated in Wichman [21]. This experimental flame temperature varies with the free-steam oxidizer mass fraction. The value of the fuel mass fraction in the fuel stream was 0.85. The flame temperatures are correlated with a fourth-order polynomial as

$$T_f = 486.66 + 12230.85\,Y_{OO} - 25728.64\,Y_{OO}^2 + 25360.02\,Y_{OO}^3 - 9323.0\,Y_{OO}^4.$$

We calculate $Q_F = 49{,}986$ kJ/kg from the expression for T_f in the Nomenclature using $Y_{OO} = 0.211$, $Y_{FF} = 0.85$ and $T_O = 298$ K. This is within 10% of the experimental value for methane. We wish to employ physical parameters that nominally resemble those for representative hydrocarbons. The modified formula

† Soot research has become a subject largely unto itself with the goal of understanding soot properties, morphology, optical response, etc. [2]. The objective of such work is to generate fundamental understanding of soot characteristics. The synthesis of results of soot research into a comprehensive account of the problem from whence it originally arose, flame theory, has not yet occurred.

$$T_f = T_o + \frac{Q_F Y_{FF} f(Y_{oo})}{C_p(1+\phi)}, \quad f = \frac{5}{4}\exp(-3Y_{OO}) + \frac{1}{3}, \qquad (1)$$

correlates the previous T_f expression identically when $Y_{FF} = 0.85$, see Fig. 2. The Y_{FF} values corresponding to the different curves in the plot range from 0.25 (lowest) to 1.0 (highest). We note that for Y_{FF} values of 0.25 and 0.30, however, the peak flame temperature does not occur at $Y_{OO} = 1$. There is a slight local maximum in between. Our cutoff value is $Y_{FF} = 0.30$, below which we make no calculations. Except for highly sooting species, this cutoff is realistic because a low Y_{FF} generally does not produce sooty flames.

The parameter values of Tzeng et al. [22] were used. These are $c_p = 1.35$ kJ/kg-K, $\alpha = 1.24 \times 10^{-4}$ m^2/s, $\nu = 4.0$, $A = 5 \times 10^7$ s^{-1}, $E = 121{,}940$ kJ/kmol.

We write the equations and boundary conditions for conservation of energy and species. In nondimensional form, these are

$$\frac{\partial \tau}{\partial \bar{t}} = \frac{1}{\bar{s}_0^2}\frac{\partial^2 \tau}{\partial Z^2} + \bar{Q}_F \mathbf{D}r + N_R \frac{dq_R}{dZ}, \qquad (2.i)$$

$$\frac{\partial y_o}{\partial \bar{t}} = \frac{1}{\bar{s}_0^2}\frac{\partial^2 y_o}{\partial Z^2} - \phi \mathbf{D}r, \qquad (2.ii)$$

$$\frac{\partial y_F}{\partial \bar{t}} = \frac{1}{\bar{s}_0^2}\frac{\partial^2 y_F}{\partial Z^2} - \mathbf{D}r. \qquad (2.iii)$$

This model is chosen for many reasons. First, it contains all of the terms that describe flame responses to heat losses. Second, it is generically similar to all diffusion flames into which our one-dimensional model variant topologically maps [equations (2) are the same *with* a convective flow]. Third, the Damköhler number contains all of the relevant parameters including reaction time and diffusion time, $t_{ref} = L^2/\alpha_o$. Fourth, a detailed mass-loss term from the fuel equation is unnecessary if we postulate (in agreement with experimental results [1]) that only a trace amount of the gaseous fuel forms soot. Finally, one-step chemistry is employed because a universally accepted multi-step flame chemistry model does not exist which describes the accretion of the fuel into a soot conglomerate. Numerous alternatives are available [23, 24].

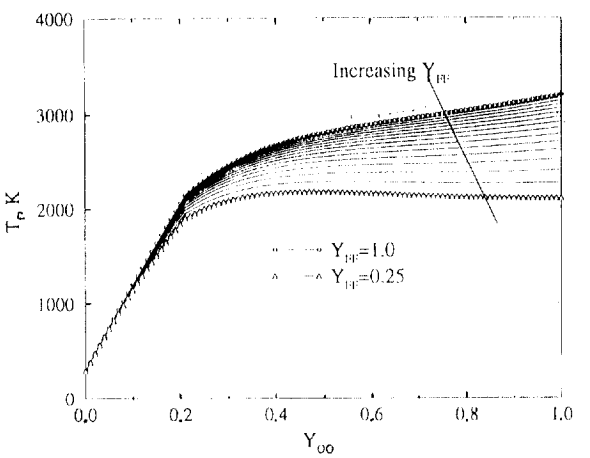

Fig. 2. Flame temperatures via simple correlation.

It is important to point out here that the purpose of this work is not to simulate a diffusion flame and obtain agreement with experimental data. Rather, we examine the sensitivity of a given reaction zone (flame) to a systematic variation of an imposed heat loss profile. Hence, the intensity, width and location of the heat loss zone are parametrically varied for each chosen flame (corresponding to prescribed oxidizer and fuel mass fractions in the respective reservoirs). In particular, we are interested in the effect on the total heat release q_{Total}, the heat flux to the reservoir walls, the radiative fraction and the drop in flame temperature as the loss zone parameters are varied. Emphasis is laid on establishing the extinction criteria for a given diffusion flame weakened sufficiently by severe heat losses. Note that if soot chemistry and the associated radiation effect are included, by assuming a soot mechanism and a radiation model, then a given flame will have a unique radiation loss profile. There is no longer an opportunity for investigating how weak the flame becomes with increased heat losses. Hence, we deliberately assume a heat loss function which is not coupled to either the energy or the species equations. As we subsequently show, there is a simple way of assessing the radiation number N_R for a realistic sooty flame. Based on our understanding of the sensitivity of the chosen flame to a heat loss, we can then say how strongly the flame will be influenced by the loss zone with the calculated N_R value. Recall also that our loss zone can alternatively be considered as a radiating porous grid placed next to a flame. In that situation, even for a given flame, for grids of different materials and porosities placed at various distances from the flame, the radiation loss term can vary significantly. We may also alternatively consider two different fuel–oxidizer combinations which produce approximately the same reactivity profile (flame) but have different sooting profiles and hence, different heat loss zones.

For our numerically-computed solutions, the initial conditions are identical to those for an infinite reaction rate (IRR), Burke–Schumann flame. We integrate our equations to a steady-state, if one exists. Shown in Figs 3(a),(b) are representative numerically-determined temperature and reactivity profiles for the indicated parametric values. These figures will be discussed in Section 5.

2.1. Heat loss profile

We shall examine two kinds of heat loss functions. The first is the top-hat profile, for which

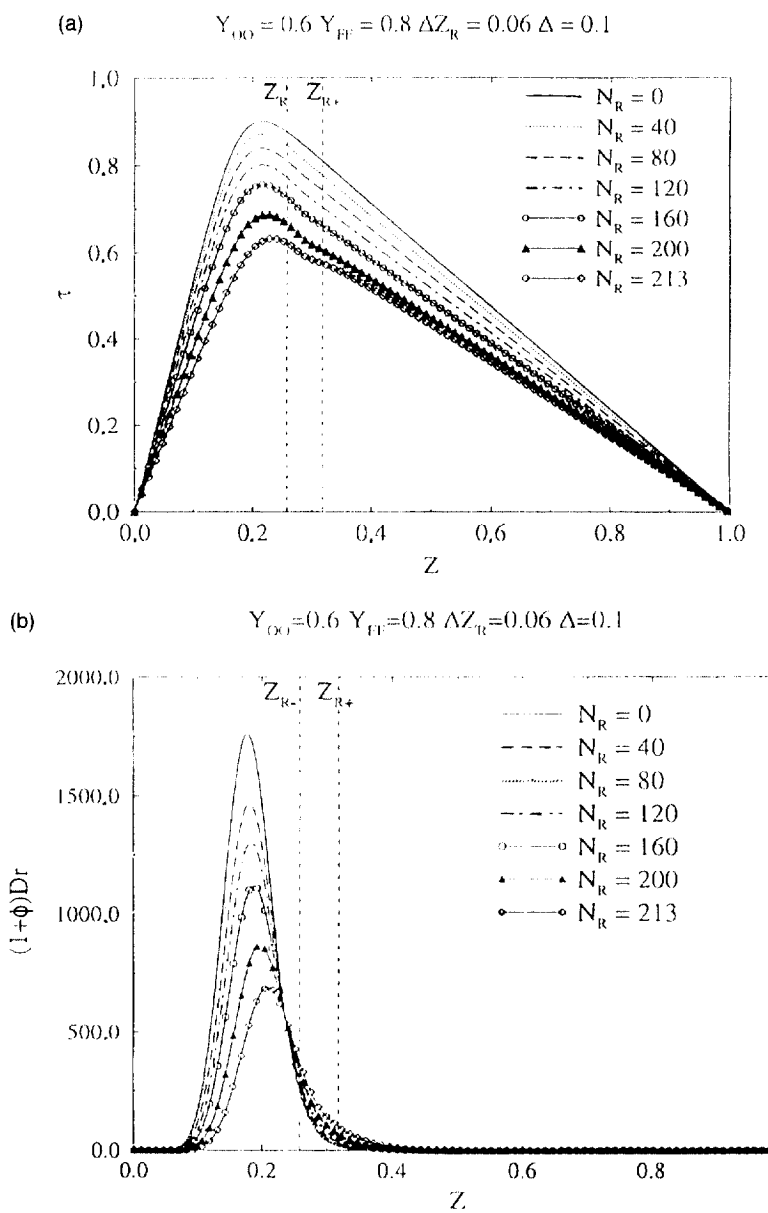

Fig. 3. (a) The influence of N_R on the temperature profile. The loss zone is located between Z_{R-} and Z_{R+}. Note the local dip in the temperature profile in the loss zone and the movement of the temperature peak toward the fuel side for increased N_R values. (b) The influence of N_R on the reactivity profile. Notice the movement of the profile toward the fuel side for increased N_R values.

$$-\frac{d\bar{q}_R}{dZ} = U(Z_{R-}) - U(Z_{R+}) \tag{3}$$

with $\Delta Z_R = Z_{R+} - Z_{R-}$ the width of the heat loss profile in the mixture fraction space. This heat loss profile is used in the analytical solution of the problem with asymptotic methods. Although quite simple, this function, however, is non-continuously differentiable at Z_{R-} and Z_{R+}, and is not suitable for a numerical solution. For this reason, we shall employ the second heat loss function,

$$-\frac{d\bar{q}_R}{dZ} = \operatorname{sech}^2[B(Z - Z_R)], \tag{4}$$

which is centered at $Z = Z_R$. The width of this loss zone depends on the magnitude of parameter B. It is clear that the loss term can be modified by changing the value of the radiation number, N_R and the width of the loss zone. At this stage we define Δ as the separation distance of the loss zone from the Burke–Schumann theoretical flame location Z_f, i.e. $\Delta = Z_{R-} - Z_f$. Thus, N_R, ΔZ_R and Δ can

be parametrically varied to examine the influence of the heat loss profile on a diffusion flame.

The integrated value of the top-hat loss profile is $\int_0^1 N_R(U(Z_{R-})-U(Z_{R+}))dZ = N_R\Delta Z_R$. For the sech^2 profile the integrated heat loss is given by

$$\int_2^1 \mathrm{sech}^2[B(Z-Z_R)]dZ = (2N_R/B)[1/(1+\exp(-2BZ_R)) - 1/(1+\exp(2B(1-Z_R)))].$$

For large B this equals $2N_R/B$ showing that the width of the sech^2 function can be written as $\Delta Z_R = 2/B$ in direct analogy with the top-hat profile.

There is, of course, no feature of the sech^2 profile that could not be equally satisfied with a Gaussian or another profile. Each is characterized by an amplitude and a width. Identical methods are used in turbulence, where PDFs are employed in physically-meaningful integrals. Integrands involving moments, PDFs and other distributions need not be defined with precision, because they shall be integrated and smoothed. The differentiability properties of the sech^2 profile become advantageous in a numerical analysis.

3. Theoretical solution

Here we examine equations (2) without the transient terms, along with equation (3) for the loss term.

We first develop an expression for the radiant loss amplitude, $N_R = q_{R\mathrm{ref}}/[\lambda_o(T_f-T_o)/L]$. We employ the physical formula for optically thin materials, $dq_R/dx = 4a_p\sigma(T^4-T_o^4)$, with $a_p = 1864.32 f_v T$ (m^{-1}) [25]. We replace T by T_R, the characteristic gas temperature in the loss zone (at Z_R, say), and we write $f_v = f_{vR}[U(Z_{R-})-U(Z_{R+})]$. Then (see [25] for details)

$$N_R = 7457.28\frac{\sigma T_R(T_R^4-T_o^4)f_{vR}L^2}{(\rho_R/\rho_o)\lambda_o(T_f-T_o)}\bar{s}_o, \tag{5}$$

where $\bar{s}_o = s_o/\rho_o L$. To find the magnitude of this non-dimensional expression, we may use $T_f = 1700$ K, $T_R = 1500$ K, $f_{vR} = 1\times10^{-5}$ to find $N_R = 57\bar{s}_o$. Since $\bar{s} = O(10^{-1})$, we see that N_R is between $O(1)$ and $O(10)$. This estimate is in order-of-magnitude agreement with the radiant loss term in a full flame/soot/radiation model that includes nucleation, coagulation, oxidation, convection, etc. [25].

We develop the solution of the equations for extinction. The details are provided in [25]. Application of activation-energy asymptotics (AEA) yields an upper bound for the total energy lost from the radiant-loss zone,

$$N_R\Delta Z_R = \frac{1}{Z_f(1-\theta/2)\beta}\ln\left[\frac{4\mathbf{D}\bar{s}_o^2Z_f^2(1-Z_f)^3}{b_E^3\beta^3}\right], \tag{6}$$

where

$$b_E = \{e[(1-|a|)-(1-|a|)^2+0.26(1-|a|)^3 + 0.055(1-|a|)^4]\}^{1/3},$$

$$a = 2Z_f-1.$$

The relationship between the value of the Damköhler number at extinction with no heat losses, and the Damköhler number at extinction with heat losses, is

$$\mathbf{D}_E = \mathbf{D}_E^*[\exp|h_o|]^n, n = Z_f/Z_{R-} < 1, \tag{7}$$

where

$$h_o = \beta H(Z_{R-}) = \beta[\tau(Z_{R-})+y_O(Z_{R-})+y_F(Z_{R-})-1]. \tag{8}$$

The quantity $H(Z_{R-})$ is the enthalpy function, evaluated at Z_{R-}. We note that the flame and soot-zone locations are assumed in the analysis not to overlap. That is, $n = Z_f/Z_{R-}$ is always less than unity. Because $y_F(Z_{R-})$ is smaller than unity and $y_O(Z_{R-})$ is nearly zero, $h_o \simeq \beta[\tau(Z_{R-})-1]$. We may estimate $\tau(Z_{R-}) \simeq \tau_R$. Equation (7) shows that the extinction Damköhler number with losses is considerably higher than without losses, and that the closer the flame and loss zone become (i.e., the closer n approaches to unity) the larger is $\mathbf{D}_E$ relative to $\mathbf{D}_E^*$. Because the flame with radiant losses extinguishes at a higher Damköhler number, it is easier to extinguish.

A comparison of equation (6) with numerically calculated extinction results is shown in Fig. 4(a). The total radiative energy loss increases as Z_f decreases for a fixed value of Y_{OO}, i.e., as Y_{FF} increases. The difference between the analytical and numerical solutions at first glance suggests poor agreement. However, closer scrutiny reveals that the analytical extinction values are $3.84\pm1.5\%$ times those obtained from the numerical solution, where the $\pm1.5\%$ error is an RMS measure. Since Y_{OO} was fixed, we anticipate that the correction factor will depend upon Y_{OO}. The analytical formula (6) was derived using asymptotic methods of analysis subject to various restrictions that are not realized in practice. The most severe restriction is the required complete separation between the flame and soot layer which, as shown in Fig. 3(a), is not observed, even when $N_R = 40$. As N_R increases, the overlap becomes more pronounced. The strong sensitivity of the diffusion flame to heat losses may explain the relative largeness of the required multiplicative factor of $(3.84)^{-1}$.

Other results can be derived from the top-hat model. We shall see in sections 4, 5 that for most conditions of overall stoichiometry, heat loss intensity, separation distance, and loss-zone width, the location of the reaction-zone peak can shift from its original position near Z_f. The shift is usually toward the loss zone. A qualitative explanation of this behaviour is provided in [24], where it is shown that in many cases DF survival is enhanced as the reaction zone moves toward the loss zone.

4. Numerical solution

The governing equations (2) were solved subject to placement of the loss zone, initial conditions for the BS

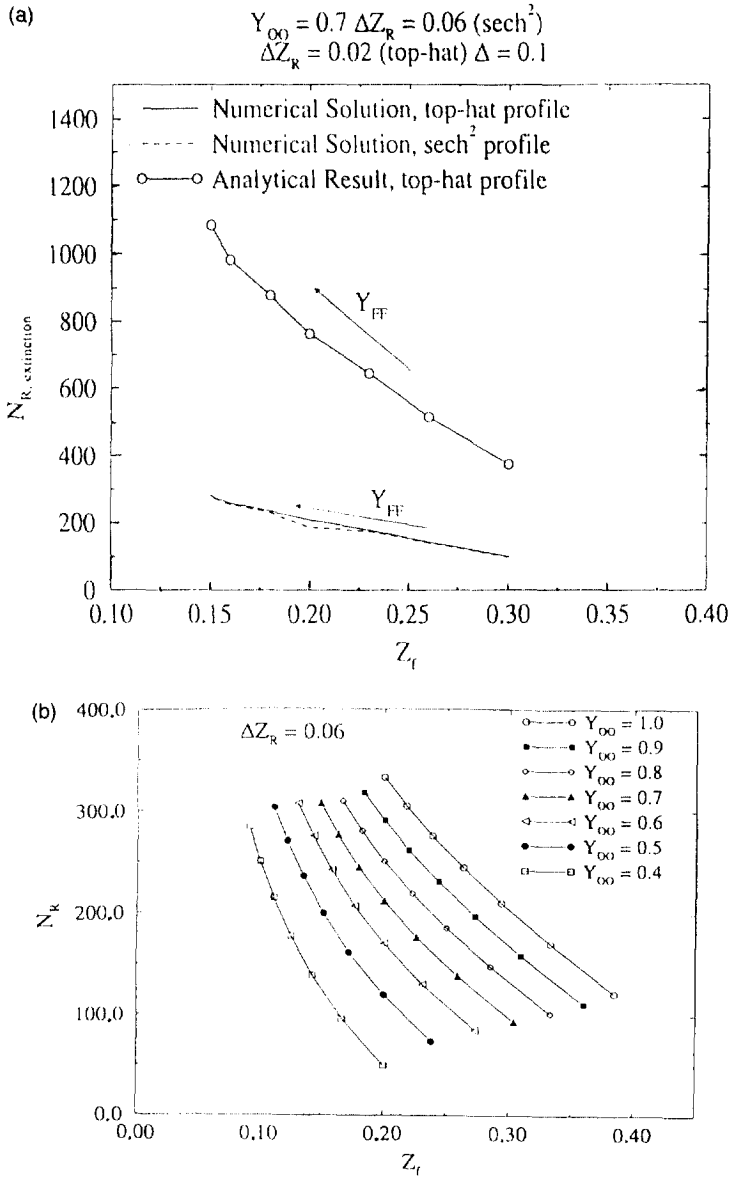

Fig. 4. (a) Plot of $N_{R,extinction}$ versus Z_f for the top-hat loss profile. (b) Extinction plot for $\Delta Z_R = 0.06$ and zero initial displacement, $\Delta = 0$ for the sech^2 loss profile. Along each curve, Y_{FF} increases as Z_f decreases. the largest Y_{FF} values have the highest $N_{R,extinction}$ values.

flame, and the boundary conditions indicated in Fig. 1. A standard implicit finite difference scheme was used in which the nonlinear terms were linearized using Newton's method. For each time step, iterations were employed until the sum of the normalized residuals fell below 1E-6. The transient conservation equations (2) were integrated to a steady state. These solutions were checked in some cases with a shooting algorithm that employed only the steady-state equations. In general, the unsteady solution was more robust. The shooting approach required nearly perfect initial conditions, without which it would diverge to a non-physical solution. Existence and uniqueness of solutions was not proved for the system of equations (2).

In the rendering of our solutions into physical coordinates, we evaluate the transformation factor $\bar{s}_o$, which

depends on the density profiles. An iterative process is required. We use the ideal gas law to derive the following relation between $\bar{\rho}$ and τ [24, 25],

$$\bar{\rho} = \frac{1-\alpha}{1-\alpha(1-\tau)}.$$

For the ambient surroundings, $\tau = 0$ and $\bar{\rho} = 1$. At the flame temperature the nondimensional density is $\bar{\rho} = 1-\alpha$. In the numerical solution, we must evaluate $\bar{s}_0$ at every time step. It can be shown that

$$\bar{s}_0 = \frac{1}{\int_0^1 \frac{1}{\rho} dZ} = \frac{1}{1+(\alpha/(1-\alpha))\int_0^1 \tau dZ}.$$

The relation between $\bar{x}$ and Z is

$$\bar{x} = \frac{\int_Z^1 (1/\bar{\rho}) dZ}{\int_0^1 (1/\bar{\rho}) dZ}.$$

From equations (2), the solutions in Z can be transformed to the physical coordinate $\bar{x}$. The quantity $\bar{s}_0$ is evaluated once the density distribution is known: the limits $(1-\alpha) \leqslant \bar{s}_0 \leqslant 1$ must be obeyed.

5. Results and discussion

Figure 3(a) depicts the nondimensional temperature, τ, plotted as a function of the mixture fraction coordinate, Z, for different values of the radiation number, N_R, for the parameter values shown. In our subsequent analysis, we retain the same set of (Y_{OO}, Y_{FF}) and vary the location, width and intensity of the radiative loss zone. The trends for other sets of reservoir mass fraction values are similar. The flame temperature profile is uniformly lowered as N_R increases. The flame temperature peak moves toward the fuel side. The drop in the peak temperature, as well as the shift of the peak, becomes more prominant for higher N_R values. For N_R greater than 213, we no longer obtain a steady state temperature profile, indicating radiative extinction. This upper bound is defined as $N_{R,extinction}$. We also note that there is a local dip of the temperature profile in the radiative loss zone for higher values of N_R.

Figure 3(b) shows the nondimensional reaction rate term for the same case. The reaction rate profile collapses for increasing N_R values. The reaction rate peak moves towards the fuel side. This movement is more conspicuous for higher values of N_R. The reaction rate peak is always to the left of the temperature peak, i.e., $Z_f < Z_r < Z_\tau$. This behaviour is in accordance with the results obtained for pure diffusion flames without radiative losses [4].

Figure 4(b) is an extinction plot for the case when $\Delta Z_R = 0.06$ and $\Delta = 0$ (i.e., zero initial separation). Extinction values of N_R are plotted as a function of Z_f, the theoretical flame location in mixture fraction coordinate. For a given value of the oxidizer mass fraction at the wall, $(N_R)_{extinction}$ increases as Z_f is decreased. A decrease in Z_f implies, for fixed Y_{OO}, an increase in Y_{FF}. As Y_{FF} increases, the reaction rate becomes more vigorous; it becomes more difficult to extinguish the flame through radiative losses. For the same value of Z_f, a lower value of Y_{OO} means a correspondingly smaller value of Y_{FF}. The reaction rate diminishes, making it easier to extinguish the flame. This explains the leftward shift for decreasing values of Y_{OO}.

We next examine some quantities of practical interest. We retain $Y_{OO} = 0.6$ and $Y_{FF} = 0.8$ with different thicknesses of the radiative loss zones and for different separation distances. The flame transfers heat to the oxidizer wall by conduction and radiation, hence $Q_{W,O} = Q_{W,O,cond} + Q_{W,O,rad}$. Half of the radiative losses travel to each wall in the thermally-thin limit. We transform the expressions for $Q_{W,O,cond}$ and $Q_{W,O,rad}$ to the Z coordinate and normalize $\bar{Q}_{W,O} = (1/\bar{s}_0)(d\tau/dZ)|_{Z=0} + 0.5 \times N_R \int_0^1 (1/\bar{s}_0)(d\bar{q}_R/dZ) dZ$. When $\bar{Q}_{W,O}\bar{s}_O$ is plotted it is seen that the global, integrated heat transfer characteristics do not depend strongly on the separation distance Δ. We obtain distinct groups of curves which correspond to different loss zones of different thicknesses. However, Δ does become important for higher values of N_R close to extinction. Also, the value of N_R required for extinction is higher when the heat loss zone is very thin, as intuitively obvious.

We plotted $\bar{Q}_{W,O}\bar{s}_O$ as a function of $N_R(2/B)$. Figure 5(a) shows that the quantity $N_R(2/B)$, which is approximately the value of the total heat loss integral $\int_0^1 N_R \operatorname{sech}^2[B(Z-Z_R)]dZ$, collapses the wall heat transfer data except very near extinction. When plotted against $N_R(2/B)$, $\bar{Q}_{W,O}\bar{s}_0$ does not reveal any appreciable dependence on either the separation distance or the thickness of the loss zone. It is also apparent from Fig. 5(a) that for high values of N_R near extinction the heat loss to the oxidizer wall decreases and the curves become distinguishable from one another.

Another quantity of practical interest is the radiative fraction χ, given by the ratio q_{Rad}/q_{Total}. The quantity q_{Total} decreases with increasing values of N_R, as seen in Fig. 5(b). For thicker loss zones, the drop in q_{Total} with increasing values of N_R is more rapid. We plot the total heat release q_{Total} as a function of $N_R(2/B)$, as shown in Fig. 6(b). The curves for different loss zone thicknesses collapse onto one another except near extinction.

The variation of χ as a function of N_R for different thicknesses of the loss zones and for $\Delta = 0$ can be evaluated. Here, χ increases with increasing N_R for a flame with a given loss zone thickness. The integrated quantity q_{Rad} increases with N_R and, because q_{Total} decreases, χ, which is a ratio of the above quantities, increases. In order to produce a given value of χ, a higher N_R is required for a flame with a thinner loss zone. We plot χ as a function of $N_R(2/B)$ in Fig. 6(a), which again indicates that the integrated heat loss characterizes the radi-

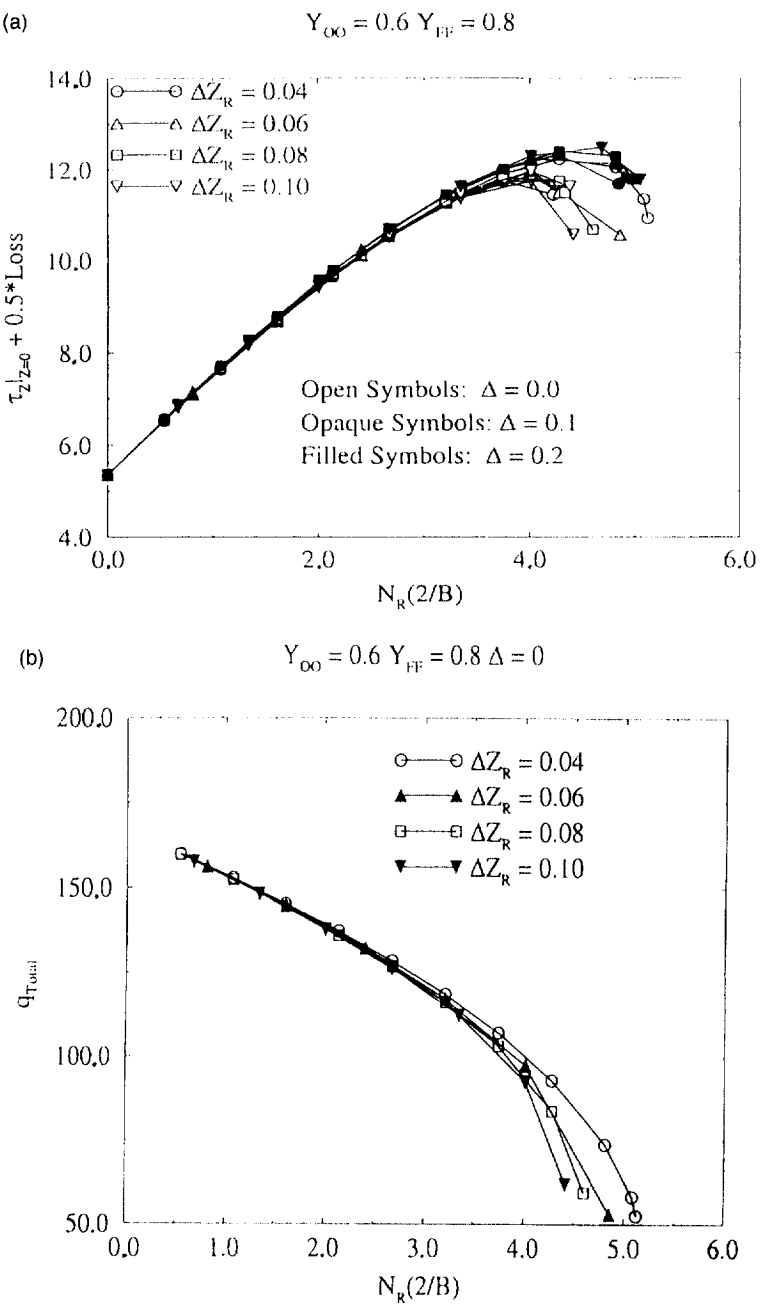

Fig. 5. (a) A plot of total nondimensional heat flux to the oxidizer wall versus abscissa $N_R(2/B)$. The correlation of the straight-line region is (heat flux) $= 1.9N_R(2/B) + 5.3$. (b) Plot of the total heat release as a function of $N_R(2/B)$ shows collapse of the data to a single line except very near extinction.

ative fraction very well, except near extinction. The limiting value of χ for which extinction occurs ranged between ~ 0.28 ($\Delta Z_R = 0.10$) and ~ 0.36 ($\Delta Z_R = 0.04$).

Figure 6(b) shows the variation of the drop in flame peak temperature, $\Delta\tau_f$, as a function of the radiative fraction χ. If we denote the maximum temperature by τ_f, then $\Delta\tau_f$ is defined as $1 - \tau_f$. We recall the temperature has been normalized in such a way that the peak τ value for the IRR flame always has the value of unity, regardless of the oxidizer and fuel mass fractions. Thus, $\Delta\tau_f$ represents the drop in peak temperature for finite rate chemistry and radiative loss, in comparison to the IRR

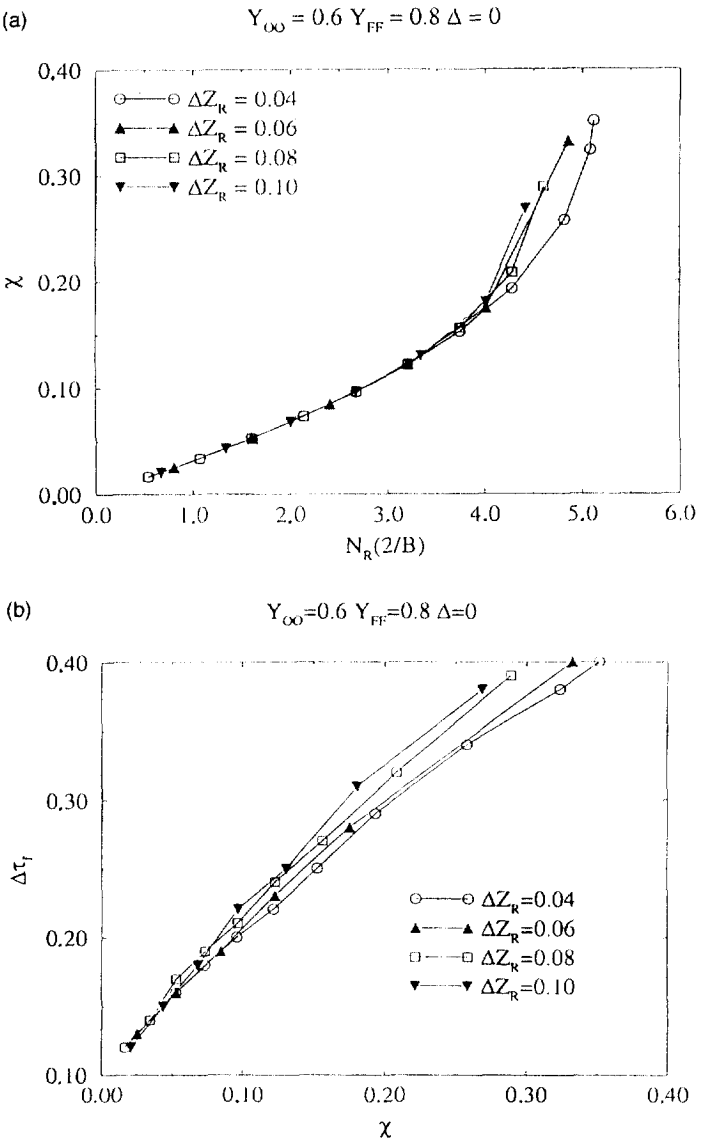

Fig. 6. (a) Radiative fraction versus $N_R(2/B)$ showing the collapse of data to a single curve. (b) The decrease in flame temperature versus radiative fraction shows a linear functional form that is virtually independent of ΔZ_R. The curves do, however, diverge from one another for high values of χ nearing extinction.

situation. The increase in $\Delta\tau_f$ with χ was almost linear for smaller values of χ. However the curves for the different loss zone thicknesses diverged from one another for higher values of χ, indicating that near extinction, flame behaviour is dependent on the thickness of the loss zones.

6. Conclusions

The following conclusions can be drawn from the present study:

1. A fuel-side heat loss zone lowers the temperature profile of a flame with a local dip observed in the zone of heat losses.
2. On increasing the heat losses, the temperature and reactivity peaks of a flame with given Y_{OO} and Y_{FF} values move toward the fuel side. For all situations, $Z_f < Z_r < Z_r$.
3. Extinction plots indicate that $N_{R,extinction}$ decreases with increased Z_f for a given Y_{OO} and, for a given Z_f, a decrease in Y_{OO} results in a decrease in $N_{R,extinction}$.
4. The heat flux to the oxidizer wall does not depend

significantly on the thickness of the loss zone or its location, and has an almost linear increase with the integrated heat loss quantity, $N_R(2/B)$. Very near extinction, however, the heat losses tend to decrease significantly.

5. The total heat release, q_{Total}, and the radiative fraction, χ, are characterized very well by the quantity $N_R(2/B)$ indicating that two heat loss zones with different intensities (N_R) and loss zone thicknesses (ΔZ_R) may have approximately the same influence on a given flame if the integrated value of the heat loss function, $N_R(2/B)$ is the same for both the loss zones.
6. The drop in peak flame temperature follows an almost linearly increasing relationship with the radiative fraction, χ, for smaller values of χ far from extinction conditions. The curves diverge from one another for higher values of χ. The extent of divergence becomes more pronounced as the extinction limit is approached.
7. An analytical formula, derived via activation-energy asymptotics (AEA), is shown to agree with our numerical results when a multiplicative numerical constant is included in the formula.

Acknowledgement

This work was funded by the NASA microgravity combustion division, contract #NAG3-1271, monitored by Kurt Sacksteder. We are very grateful for this support.

References

[1] Tien CL, Lee SC. Flame radiation. Progress in Energy and Combustion Science 1981;7:229–73.
[2] Faeth GM, Köylü ÜÖ. Structure and optical properties of flame-generated soot. In: Chan SH. editor Transport Phenomena in Combustion, Vol. 1. Washington, DC: Taylor and Francis, 1996. p. 19–44.
[3] Grosshandler WL, Modak AT. Radiation from nonhomogeneous combustion products. Eighteenth Symposium (International) on Combustion. Pittsburgh: The Combustion Institute, 1982. p. 601–9.
[4] Wichman IS. An introduction to combustion modeling using high-activation-energy asymptotic (AEA) methods. In: Puri IK. editor Environmental Implications of Combustion Processes. Boca Raton: CRC Press, 1993: p. 139–83.
[5] Chen JM, Card JM, Day M, Mahalingam S. Direct numerical simulation of turbulent non-premixed methane–air flames. In: Chan SH. editor Transport Phenomena in Combustion, Vol. 2. Washington, DC.: Taylor and Francis, 1996. p. 1049–60.
[6] Williams FA. Combustion Theory, 2nd edition. Menlo Park, CA: Benjamin/Cummings, 1985. p. 78.
[7] Syed KJ, Stewart CD, Moss JB. Modeling soot formation and thermal radiation in buoyant turbulent diffusion flames. Twenty-Third Symposium (International) on Combustion. Pittsburgh: The Combustion Institute, 1990. p. 1533–41.
[8] Kennedy IM, Kollman W, Chen JH. A model for soot formation in a laminar diffusion flame. Combustion and Flame, 1990;81:73–85.
[9] Leung KM, Lindstedt RP, Jones WP. A simplified reaction mechanism for soot formation in non-premixed flames. Combustion and Flame 1991;87:289–305.
[10] Ku JC, Tong L, Greenberg PS. Measurements and modeling of soot formation and radiation in microgravity jet diffusion flames. HTD-Vol. 335, Proceedings of the ASME Heat Transfer Division, 1996;4, p. 261–70.
[11] Hsu P-F, Ku JC. Radiative heat transfer in finite cylindrical enclosures with nonhomogeneous participating media. J. Thermophys. Heat Transfer 1994;8:434–40.
[12] Bressloff JB, Moss JB, Rubini PA. CFD prediction of coupled radiation heat transfer and soot production in turbulent flames. Twenty-Sixth Symposium (International) on Combustion. Pittsburgh: The Combustion Institute, 1996. p. 2379, 2386.
[13] Beck JV, Arnold KJ. Parameter Estimation in Engineering and Science. New York: Wiley, 1977. p. 17–23.
[14] Scott EP, Beck JV. Estimation of thermal properties in carbon/epoxy composite materials during curing. Journal of Composite Materials 1992;1(26):20–35.
[15] Fureby C, Lundgren E, Möller S-I. On the formation of the governing equations of combustion systems. In: Chan SH. editor Transport Phenomena in Combustion, Vol. 2. Washington DC.: Taylor and Francis, 1996. p. 909–920.
[16] Lees JC, Yetter RA, Dryer FL. Transient numerical modeling of carbon particle ignition and oxidation. Combustion and Flame 1995;101:387–98.
[17] Panagiotou T, Levendis Y, Delichatsios M. Measurements of particle flame temperatures using three-color optical pyrometry. Combustion and Flame 1996;104:272–87.
[18] Sunderland PB, Faeth GM. Soot formation in hydrocarbon/air laminar jet diffusion flames. Combustion and Flame 1996;105:132–46.
[19] Ray SR. Flame spread over solid fuels. PhD thesis. Princeton University, Princeton, NJ, 1981.
[20] Fernandez-Pello AC, Ray SR, Glassman I. Flame spread in an opposed forced flow: the effect of ambient oxygen concentration. Eighteenth Symposium (International) on Combustion. Pittsburgh: The Combustion Institute 1980. p. 579–87.
[21] Wichman IS. Studies of flame spread in an opposed flow over surfaces of solid fuels. PhD thesis. Princeton University, Princeton, NJ, 1983.
[22] Tzeng LS, Atreya A, Wichman IS. A one-dimensional model of piloted ignition. Combustion and Flame 1980;80:94–107.
[23] Bockhorn H. Soot Formation in Combustion: Mechanisms and Models. Berlin: Springer-Verlag, 1994.
[24] Frenklach M, Wang H. Detailed modeling of soot particle nucleation and growth. Twenty-Third Symposium (International) on Combustion. Pittsburgh: The Combustion Institute, 1990. p. 1559–66.
[25] Wichman IS, Ray A. Influence of a simple heat loss profile on a pure diffusion flame. MSU technical report in Mechanical Engineering, MSU CRL 07-29-96, Michigan State University, East Lansing, MI, 1996.
[26] Ray A. Theoretical and numerical investigation of radiative extinction of diffusion flames. PhD thesis. Michigan State University, East Lansing, MI, 1996.